Outage Analysis of the Hybrid Free-Space Optical and Radio-Frequency Channel

Nick Letzepis, *Member, IEEE*, Khoa D. Nguyen, *Student Member, IEEE*,
Albert Guillén i Fàbregas, *Senior Member, IEEE*, and William G. Cowley, *Member, IEEE*

***Abstract*—We study the hybrid free-space optical (FSO) and radio-frequency (RF) channel from an information theoretic perspective. Since both links operate at vastly different carrier frequencies, we model the hybrid channel as a pair of parallel channels. Moreover, since the FSO channel signals at a higher rate than the RF channel, we incorporate this key feature in the parallel channel model. Both channels experience fading due to scintillation, which is slow compared to typical signalling rates. Under this framework, we study the fundamental limits of the hybrid channel. In particular, we analyse the outage probability in the large signal-to-noise ratio (SNR) regime, and obtain the outage diversity or SNR exponent of the hybrid system. First we consider the case when only the receiver has perfect channel state information (CSIR case), and obtain the exponents for general scintillation distributions. These exponents relate key system design parameters to the asymptotic outage performance and illustrate the benefits of using hybrid systems with respect to independent FSO or RF links. We next consider the case when perfect CSI is known at both the receiver and transmitter, and derive the optimal power allocation strategy that minimises the outage probability subject to peak and average power constraints. The optimal solution involves non-convex optimisation, which is intractable in practical systems. We therefore propose a suboptimal algorithm that achieves significant power savings (on the order of tens of dBs) over uniform power allocation. We show that the suboptimal algorithm has the same diversity as the optimal power allocation strategy.**

I. Introduction

In free-space optical (FSO) communication an optical carrier is employed to convey information wirelessly. FSO systems have the potential to provide fiber-like data rates with the advantages of quick deployment times, high security and no frequency regulations. Unfortunately such links are highly susceptible to atmospheric effects. *Scintillation* induced by atmospheric turbulence causes random fluctuations in the received irradiance of the optical laser beam [1]. Numerous studies have shown that performance degradation caused by scintillation can be significantly reduced through the use of multiple-lasers and multiple-apertures, creating the well-known multiple-input multiple-output (MIMO) channel (see e.g. [2–10]). However, it is the large attenuating effects of cloud and fog that pose the most formidable challenge. Extreme low-visibility fog can cause signal attenuation on the order of hundreds of decibels per kilometre [11]. One method to improve the reliability in these circumstances is to introduce a radio frequency (RF) link to create a *hybrid FSO/RF* communication system [11–16]. When the FSO link is blocked by cloud or fog, the RF link maintains reliable communications, albeit at a reduced data rate. Typically a millimetre wavelength carrier is selected for the RF link to achieve data rates comparable to that of the FSO link. At these wavelengths, the RF link is also subject to atmospheric effects, including rain and scintillation [17–21], but less affected by fog. The two channels are therefore complementary: the FSO signal is severely attenuated by fog, whereas the RF signal is not; and the RF signal is severely attenuated by rain, whereas the FSO is not. Both, however, are affected by scintillation.

Most works on the hybrid channel [11–14, 16] consider the RF and FSO links as separate channels, i.e. the channels do not aid each other to compensate signal level fluctuations. In these works, the main purpose of the RF link is to act as a backup when the FSO link is down. In [15] a hybrid channel coding scheme is proposed that combines both FSO and RF channels and adapts the code rate to the channel conditions. Multilevel coding schemes have also been proposed in [22] for the hybrid channel.

Lacking so far in the literature on hybrid FSO/RF channels is the development of a suitable channel model and its theoretical analysis to determine the fundamental limits of communication. This is the central motivation for our paper. We propose a hybrid channel model based on the well known parallel channel [23], and take into account the differences in signalling rate, and the atmospheric fading effects present in both the FSO and RF links. These fading effects are slow compared to typical data rates, and as such, each channel is based on a *block-fading* channel model. Previously in [2, 3], using a block-fading channel model, we examined the *outage probability* of the multiple-input multiple-output (MIMO) FSO channel under the assumption of pulse-position modulation (PPM) for several well-known scintillation distributions, i.e. lognormal, exponential, gamma-gamma, lognormal-Rice and I-K distributed scintillation [1]. In particular, we examined the *SNR exponent* (or outage diversity) [24, 25], which describes the high SNR slope of the outage probability curve when plotted on a log-log scale. In this paper, we extend this analysis to include an RF link to create a hybrid FSO/RF channel. The message to be transmitted is encoded into parallel

N. Letzepis, K. D. Nguyen and W. G. Cowley are with Institute for Telecommunications Research, University of South Australia, SPRI Building - Mawson Lakes Blvd., Mawson Lakes SA 5095, Australia, e-mail: nick.letzepis@unisa.edu.au. A. Guillén i Fàbregas is with the Department of Engineering, University of Cambridge, Cambridge CB2 1PZ, UK, e-mail: guillen@ieee.org.

This work was supported by the Sir Ross and Sir Keith Smith Fund, Cisco Systems and the Australian Research Council under RN0459498, DP0558861 and DP088160.

This paper has been presented in part at the 2009 IEEE Global Communications Conference, Honolulu, Hawaii, USA, Nov. 2009.

FSO and RF bit streams which are sent across the FSO and RF channels simultaneously. We examine the case when perfect CSI is known at the receiver only (CSIR case), then we consider the case when CSI is also known at the transmitter (CSIT case), and power allocation is employed to reduce the outage probability subject to power constraints. When CSI is not available at the transmitter, we calculate the SNR exponents of the hybrid channels for general scintillation distributions in each of the channels. On the other hand, when CSI is available at the transmitter, we derive the optimal power allocation algorithm subject to both peak and average power constraints. This optimal solution involves non-convex optimisation, which has prohibitive complexity in practical systems. We therefore propose a suboptimal solution and prove that it has the same SNR exponent as optimal power allocation.

The remainder of this paper is organised as follows. In Section II we present our channel model and assumptions. Section III reviews the required information-theoretic preliminaries. Section IV presents our main results for the CSIR-only case while Section V discusses power allocation and SNR exponents for the CSIT case. Section VI draws final concluding remarks. Proofs of our results can be found in the appendices.

II. Channel Model and Assumptions

A block diagram of the communication system of interest is shown in Fig. 1. A binary data sequence is binary encoded into parallel FSO and RF bit streams. The RF link modulates the encoded bits and up-converts the baseband signal to a millimetre wavelength RF carrier frequency. The FSO link employs intensity modulation and direct detection, i.e. information is modulated using only the irradiance of a laser beam. The RF and FSO signals are transmitted simultaneously through an atmospheric channel. The received RF signal is then downconverted to baseband and sent to the decoder. At the same time, the received irradiance is collected by an aperture, converted to an electrical signal via photodetection and sent to the decoder. The received signals are jointly decoded to recover the transmitted message.

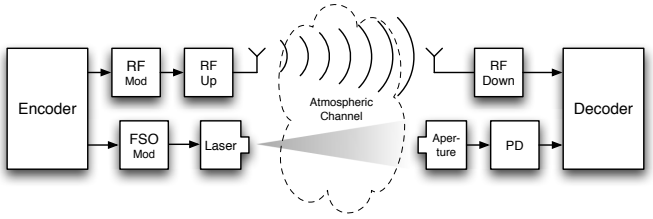

Fig. 1. Hybrid FSO/RF communication system.

In this paper we define a *hybrid channel symbol*, $(\boldsymbol{x}, \hat{x}) \in \mathcal{X}_{\text{fso}}^n \times \mathcal{X}_{\text{rf}}$, consisting of component FSO and RF symbols, which are transmitted in parallel with perfect synchronism and have the same symbol period T_s. The RF component symbol, denoted by $\hat{x}$, is drawn uniformly from an M-ary complex signal set $\mathcal{X}_{\text{rf}} \subset \mathbb{C}$ representing e.g. quadrature amplitude modulation (QAM) or phase shift keying (PSK). We assume the RF symbols are transmitted with unit average energy, i.e. $\mathbb{E}[|\hat{x}|^2] = 1$. The number of bits per RF symbol is $m \triangleq \log_2 M$ bits. Since the FSO link employs a much higher carrier frequency than the RF link, we assume the FSO component of the hybrid channel symbol consists of n symbols drawn uniformly from a constellation $\mathcal{X}_{\text{fso}}$. Most practical FSO systems employ a pulsed type of modulation, e.g. on-off keying (OOK), pulse-position modulation (PPM) or multi-PPM (MPPM). Hence we assume $\mathcal{X}_{\text{fso}}$ represents a pulse type modulation scheme, i.e. the FSO component of the hybrid symbol consists of n symbols, which are further composed of Q pulse intervals of duration T_p, where $T_s = nQT_p$. The signal set $\mathcal{X}_{\text{fso}} \subset (0,1)^Q$ is a set of Q length binary vectors, where a binary 1 at index i indicates a pulse of duration T_p in time slot i. Hence the FSO symbols $\boldsymbol{x} \in \mathcal{X}^n \subset (0,1)^{nQ}$ are $1 \times nQ$ binary vectors. We assume each T_p second 'on' pulse is normalised to have unit energy and denote the average FSO symbol energy by $\gamma = \mathbb{E}\left[\sum_{i=1}^{nQ} x_i\right]$. Let $q \triangleq \log_2(|\mathcal{X}_{\text{fso}}|)$, hence the total bits per hybrid channel symbol is $m + nq$ bits. Note that one could also consider pulse-amplitude modulated (PAM) symbols. In this case the same analysis and result that follow will apply, but for simplicity we assume on-off type pulses.

Both FSO and RF channels are affected by scintillation [1, 17–19], which is a slow fading process compared to typical data rates.[1] We therefore model each component channel by a block-fading channel model, whereby the component channels are divided into a finite number of blocks of symbols, and each block experiences an i.i.d. fading realisation. The scintillation experienced by each component channel is also assumed to be independent.[2] Typically, the RF scintillation has a coherence time on the order of seconds [17–19], whereas the FSO scintillation is much faster, having a coherence time on the order of tens of milliseconds [1]. We therefore decompose the FSO and RF components of the codeword into A and B blocks of K and L symbols respectively, where $A \geq B$. Given that the coherence time of the RF scintillation is on the order of seconds, the most realistic scenario is $B = 1$. However, for generality we will assume B is an arbitrary positive integer. Note that the total number of symbols in each FSO/RF component codeword is the same, i.e. $AK = BL$. We assume that the number of symbols in each block tends to infinity, but the ratio remains a fixed constant, i.e.

$$\lim_{K,L\to\infty} \frac{L}{K} = \frac{A}{B}. \tag{1}$$

We assume both FSO/RF component channels are modelled by independent additive white Gaussian noise (AWGN) channels. Note that this assumption for the FSO channel may not be accurate under certain conditions. The photodetector output electrical signal is proportional[3] to the incident optical irradiance waveform (instantaneous optical power).

[1] We use the terms scintillation and fading interchangeably to refer to fluctuations in power of the received FSO/RF signals.

[2] This will be true over short time intervals, but over longer time scales meteorological variations will result in correlated channel fades.

[3] The proportionality constant is referred to as the *responsivity* (measured in Watts per Ampere), and is dependent on the optical wavelength and photodetector material.

Under ideal photodetection, thermal noise is negligible and the received signal represents detected photons. The number of detected photons in a given time interval is governed by a Poisson process whose rate is proportional to the average irradiance over the time interval [26]. This is the well-known Poisson channel for which a number of works on FSO systems employ (see e.g. [7, 10, 27]). As the average irradiance increases due to increased background irradiation or high optical signal power, these statistics can be well approximated by Gaussian statistics. If avalanche photodetection is employed, then random photo-multiplication effects must be considered. A comprehensive comparison of the various photodetection models, Poisson, Webb, Gaussian (signal dependent and signal independent variations) is given in [28]. For simplicity and analytical convenience, we assume the combined shot and thermal noise can be considered as signal independent AWGN (an assumption also commonly used in the literature [1, 4, 6, 9, 26, 28, 29]). Under this assumption, the received signals can written as,

$$\boldsymbol{y}_a[k] = p_a \rho h_a \boldsymbol{x}_a[k] + \boldsymbol{z}_a[k] \tag{2}$$

$$\hat{y}_b[l] = \sqrt{\hat{p}_b \hat{\rho} \gamma \hat{h}_b} \hat{x}_b[l] + \hat{z}_b[l], \tag{3}$$

for $l = 1, \ldots, L$, $k = 1, \ldots, K$ $a = 1, \ldots, A$ and $b = 1, \ldots, B$, where: $\boldsymbol{y}_a[k] \in \mathbb{R}^{nQ}$ and $\hat{y}_b[l] \in \mathbb{C}$ are the noisy received symbols for the FSO and RF channels respectively; $\boldsymbol{x}_a[k] \in \mathcal{X}_{\text{fso}}^n$ and $\hat{x}_b[l] \in \mathcal{X}_{\text{rf}}$ denote the transmitted symbols; $\boldsymbol{z}_a[k] \in \mathbb{R}^{nQ}$ is a i.i.d. vector of zero mean unit variance real Gaussian noise, and $z_b[l] \in \mathbb{C}$ is unit variance complex Gaussian noise ($\mathcal{CN}(0,1)$); $h_a > 0$ and $\hat{h}_b > 0$ are independent random power fluctuations due to scintillation, each i.i.d. drawn from distributions f_H and $f_{\hat{H}}$ respectively, with normalisation $\mathbb{E}[h_a] = \mathbb{E}[\hat{h}_b] = 1$; p_a and $\hat{p}_b$ denotes the power of block a and b for the FSO and RF channels respectively. The γ parameter in (3) ensures both FSO and RF symbols have the same energy. The parameters $0 < \rho, \hat{\rho} < 1$ in (2) and (3) model differences in the relative strengths of the two parallel channels, e.g. it reflects long-term fading effects due to rain, fog or cloud as well as other parameters such as aperture/antenna gains and propagation loss. When $\rho > \hat{\rho}$, the FSO channel is much stronger than the RF, e.g. modelling the effects of severe rain attenuation. On the other hand, if $\rho < \hat{\rho}$, then the RF channel is stronger than the FSO channel, e.g. modelling the effects of severe fog/cloud attenuation. Although in practise ρ and $\hat{\rho}$ are randomly varying with time (and are also most likely correlated random variables), we assume they remain unchanged over many codeword time intervals and therefore are fixed constants. As we shall see later, these parameters will not affect the asymptotic outage analysis that is to follow.

In this paper, we consider two CSI scenarios. First we will assume only the receiver has perfect CSI and the transmitter allocates power uniformly across all blocks (CSIR case). Then we will consider the case where perfect CSI is also known at the transmitter (CSIT case). The transmitter then performs power allocation to reduce the outage probability subject to power constraints. The transmit power for both channels is ultimately drawn from the same power resource. As such, we assume the long-term average power consumed by the hybrid system is constrained according to

$$\mathbb{E}\left[\langle \boldsymbol{p} \rangle\right] + \mathbb{E}\left[\langle \hat{\boldsymbol{p}} \rangle\right] \leq P_{\text{av}}, \tag{4}$$

where $\langle \boldsymbol{p} \rangle = \frac{1}{A}\sum_{a=1}^{A} p_a$ and $\langle \hat{\boldsymbol{p}} \rangle = \frac{1}{B}\sum_{b=1}^{B} \hat{p}_b$. Practical communication systems have limitations on the peak power that can be transmitted. Since the FSO and RF links will realistically have different peak power limitations, we assume each is subjected to its own individual peak (or short-term) power constraint, i.e.

$$\langle \boldsymbol{p} \rangle \leq P_{\text{peak}}^{\text{fso}} \quad \text{and} \quad \langle \hat{\boldsymbol{p}} \rangle \leq P_{\text{peak}}^{\text{rf}}, \tag{5}$$

where $P_{\text{peak}}^{\text{fso}} = \alpha_{\text{fso}} P_{\text{av}}$ and $P_{\text{peak}}^{\text{rf}} = \alpha_{\text{rf}} P_{\text{av}}$ for fixed peak-to-average power ratios α_{fso} and α_{rf}.

It is important to note the difference in signal scaling between the FSO and RF AWGN channels, (2) and (3) respectively. In standard RF channels, the amplitude of the received electrical signal is proportional to the square-root of the power of the transmitted electromagnetic signal [30]. For the FSO channel, the amplitude of the received electrical signal is directly proportional to the transmitted optical power, due to the photodetection process [26]. This FSO model is slightly different to [2], where the AWGN FSO channel model was written in terms of the received electrical power (proportional to the square of the optical power). In this paper, we write the FSO AWGN channel (2) and power constraints (4) and (5) with respect to the transmitted optical and RF power. This is necessary to ensure consistency between the power constraints over the FSO and RF channels. As we shall see later, this scaling will significantly affect the design of power allocation strategies when CSI is known at the transmitter.

III. Information Theoretic Preliminaries

The channels described by (2) and (3) under the quasi-static assumption are not information stable [31] and therefore, their individual channel capacities in the strict Shannon sense are zero. For these channels, it is more appropriate to analyse the information outage probability, which lower bounds the codeword error probability of any coding scheme [32, 33]. Define the vector channel realisations $\boldsymbol{h} = (h_1, \ldots, h_A)$ and $\hat{\boldsymbol{h}} = (\hat{h}_1, \ldots, \hat{h}_B)$, and vector power allocations $\boldsymbol{p} = (p_1, \ldots, p_A)$ and $\hat{\boldsymbol{p}} = (\hat{p}_1, \ldots, \hat{p}_B)$. The total instantaneous mutual information in bits per channel use is therefore [23]

$$\begin{aligned} I_{\text{tot}}(\boldsymbol{p}, \hat{\boldsymbol{p}}, \boldsymbol{h}, \hat{\boldsymbol{h}}) = &\frac{n}{A}\sum_{a=1}^{A} I_{\mathcal{X}_{\text{fso}}}^{\text{awgn}}(h_a^2 \rho^2 p_a^2) \\ &+ \frac{1}{B}\sum_{b=1}^{B} I_{\mathcal{X}_{\text{rf}}}^{\text{awgn}}(\hat{h}_b \hat{\rho} \gamma \hat{p}_b), \end{aligned} \tag{6}$$

where $I_{\mathcal{X}}^{\text{awgn}}(u) \in (0, \log_2|\mathcal{X}|)$ denotes the input-output mutual information of the AWGN channel with input constellation $\mathcal{X}$ and SNR u. Note that the achievable rate (6) implicitly assumes joint encoding and decoding across FSO and RF channels.

The information outage probability of the hybrid system is given by

$$P_{\text{out}}(P_{\text{av}}, R) \triangleq \Pr\left\{ I_{\text{tot}}(\boldsymbol{p}, \hat{\boldsymbol{p}}, \boldsymbol{h}, \hat{\boldsymbol{h}}) < R \right\}, \tag{7}$$

where R is the target rate of the system in bits per hybrid channel use. We define the overall binary code rate of the hybrid system as $R_c \triangleq R/(m+nq)$, $0 < R_c < 1$. In addition, we define $0 < \delta < 1$ as the ratio of FSO bits to total transmitted bits, i.e. $\delta \triangleq \frac{nq}{m+nq}$.

In this paper we study the *SNR exponent* of the system, defined as

$$d^{(k)} \triangleq \lim_{P_{\rm av}\to\infty} -\frac{\log P_{\rm out}(P_{\rm av}, R)}{(\log P_{\rm av})^k}, \tag{8}$$

where $k = 1, 2$. Note that by including the integer k, (8) is more general than the SNR exponent normally defined in RF systems [24, 25]. This modified definition is required to allow for scintillation cases where the resulting outage probability curve will not converge to a constant slope when plotted on a log-log scale, but does when plotted on a $\log - \log^2$ scale (most notably under weak turbulence conditions where the scintillation is log-normal distributed [2]).

The SNR exponent will depend on the distribution of the fading coefficients. Rather than assuming a specific distribution, we characterise the fading via the component channel's single block transmission SNR exponent, defined as

$$d_{\rm fso}^{(i)} \triangleq \lim_{u\to\infty} -\frac{\log \Pr\{I_{\rm fso}^{\rm awgn}(h^2u^2) < R_{\rm fso}\}}{(\log u)^i} \tag{9}$$

$$d_{\rm rf}^{(j)} \triangleq \lim_{u\to\infty} -\frac{\log \Pr\{I_{\rm rf}^{\rm awgn}(\hat{h}u) < R_{\rm rf}\}}{(\log u)^j}, \tag{10}$$

for given component channel rate constraints $R_{\rm fso}$ and $R_{\rm rf}$, where $i, j \in \{1, 2\}$. In Table I we list some single block transmission SNR exponents (derived in [2]) for some typical scintillation distributions [1].[4] Note that the exponents derived in [2] defined the SNR exponents in terms of the received electrical SNR. In this paper, we define the FSO exponent in terms of the transmitted optical power. This results in a factor of 2 in the exponents listed in Table I compared to those given in [2].

TABLE I
SNR EXPONENTS FOR SOME TYPICAL SCINTILLATION DISTRIBUTIONS.

Distribution	PDF $f(h)$	SNR Exponent
Exponential	$\exp(-h)$	$d^{(1)} = 1$
Lognormal	$\frac{1}{h\sigma\sqrt{2\pi}} e^{-(\log h-\mu)^2/(2\sigma^2)}$	$d^{(2)} = \frac{1}{4\log(1+\sigma^2)}$
Gamma-gamma	$\frac{2(ab)^{\frac{a+b}{2}}}{\Gamma(a)\Gamma(b)} h^{\frac{a+b}{2}-1} \mathrm{K}_{a-b}(2\sqrt{abh})$	$d^{(1)} = \min(a, b)$

IV. Asymptotic Outage Analysis: CSIR case

First let us assume that perfect CSI is known only at the receiver (CSIR case). The transmitter allocates power uniformly across all blocks, i.e. $p_1 = \ldots = p_A = \hat{p}_1 = \ldots = \hat{p}_B = p = P_{\rm av}$.

[4]Note that if MIMO FSO with transmit repetition and equal gain combining is employed, then the exponents listed in Table I are simply multiplied by N_tN_r, where N_t and N_r denote the number of lasers and apertures respectively [2].

Theorem 4.1: Define component channel SNR exponents $d_{\rm fso}^{(i)}$ and $d_{\rm rf}^{(j)}$ as in (9) and (10) respectively. Suppose $\rho, \hat{\rho} > 0$ and $i = j = k$. Then the SNR exponent is given by

$$d^{(k)} = \inf_{\mathcal{K}(\delta,R_c)} \left\{ d_{\rm fso}^{(k)}\kappa_1 + d_{\rm rf}^{(k)}\kappa_2 \right\}, \tag{11}$$

where

$$\mathcal{K}(\delta, R_c) \triangleq \Big\{ \kappa_1, \kappa_2 \in \mathbb{Z} : \delta\frac{\kappa_1}{A} + (1-\delta)\frac{\kappa_2}{B} > 1 - R_c, \\ 0 \le \kappa_1 \le A, 0 \le \kappa_2 \le B \Big\}. \tag{12}$$

Proof: See Appendix A. ∎

From Theorem 4.1, we see that the overall SNR exponent depends on R_c, δ, A, B and the individual SNR exponents $d_{\rm fso}$ and $d_{\rm rf}$ in a non-trivial way. Although in general, the solution to (11) can be straightforwardly determined numerically, it is difficult to obtain insight as to how the various system parameters influence the overall SNR exponent. However, for the most basic and interesting scenario, $A = B = 1$, the solution to (11) reduces to a simple intuitive form.

Corollary 4.1: Suppose $A = B = 1$. The solution to (11) is divided into two cases as follows.

1) If $\delta \le \frac{1}{2}$, then

$$d^{(k)} = \begin{cases} d_{\rm fso}^{(k)} + d_{\rm rf}^{(k)} & 0 < R_c \le \delta \\ d_{\rm rf}^{(k)} & \delta < R_c \le 1-\delta \\ \min(d_{\rm fso}^{(k)}, d_{\rm rf}^{(k)}) & 1-\delta < R_c < 1. \end{cases} \tag{13}$$

2) If $\delta \ge \frac{1}{2}$, then

$$d^{(k)} = \begin{cases} d_{\rm fso}^{(k)} + d_{\rm rf}^{(k)} & 0 < R_c \le 1-\delta \\ d_{\rm fso}^{(k)} & 1-\delta < R_c \le \delta \\ \min(d_{\rm fso}^{(k)}, d_{\rm rf}^{(k)}) & \delta < R_c < 1. \end{cases} \tag{14}$$

Proof: See Appendix B. ∎

From Corollary 4.1 we can see directly how the hybrid system parameters will affect the asymptotic slope of the outage probability curve for the single block transmission case. In particular, we see that the asymptotic slope is affected by the SNR exponent of the individual component channels (which is in turn dependent on the scintillation distribution), the size of the FSO/RF signal set constellation, and the overall binary code rate of the system. In most practical systems, $\delta \ge \frac{1}{2}$, i.e. in a hybrid symbol period, the number of transmitted FSO bits will be greater than the number of RF transmitted bits. From (14), we see that the highest diversity is achieved if the binary code rate R_c is set to be less than $1-\delta = m/(m+nq)$, i.e. the total information rate is less than the maximum information rate of the stand-alone RF channel. If $1-\delta < R_c \le \delta$, the exponent is the same as a single FSO link, i.e. the additional coding over an RF link will not improve the asymptotic slope of the outage probability curve. For high binary code rates, $\delta < R_c < 1$, the asymptotic performance is dominated by the worst of the two exponents. Note that code rates above δ are not achievable with a stand-alone FSO link.

Although we have concentrated on the single block case, given the short coherence time of the optical channel compared to the RF channel, the cases of $A = 2, 3$ and $B = 1$ are also of practical interest and are readily evaluated from Theorem

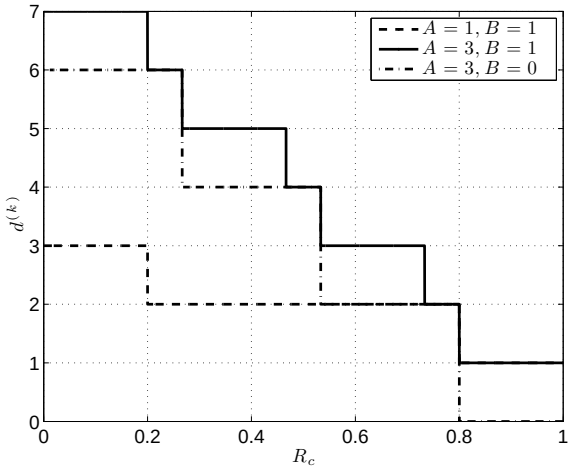

Fig. 2. Hybrid channel SNR exponent (11) with $d_{\text{fso}}^{(k)}=2$, $d_{\text{rf}}^{(k)}=1$ and $\delta=0.8$: $A=1$, $B=1$ system (dashed line); $A=3$, $B=1$ system (solid line); and a stand-alone FSO link with three blocks, i.e. $A=3$, $B=0$ (dot-dashed line).

4.1. In particular, these provide significant SNR exponent improvements for lower rates, compared to the single block case. This is illustrated in Fig. 2, which plots the hybrid channel SNR exponent with, $d_{\text{fso}}^{(k)}=2$, $d_{\text{rf}}^{(k)}=1$ and $\delta=0.8$ for a: $A=1$, $B=1$ system (dashed line); $A=3$, $B=1$ system (solid line); and a stand-alone FSO link with three blocks[5], i.e. $A=3$, $B=0$ (dot-dashed line). By coding over more FSO blocks, vast improvements in the SNR exponent can be seen, particularly as the code rate decreases. In addition, we see that the $A=3$, $B=1$ exponent exceeds that of the stand-alone FSO system by $d_{\text{rf}}^{(k)}$ for most code rates.

Theorem 4.2: Define component channel SNR exponents $d_{\text{fso}}^{(i)}$ and $d_{\text{rf}}^{(j)}$ as in (9) and (10) respectively. Suppose $i>j$ then the SNR exponent is

$$d^{(i)}=d_{\text{fso}}^{(i)}\left(1+\left\lfloor\frac{A}{\delta}\left(\delta-R_c\right)\right\rfloor\right) \qquad 0<R_c\leq\delta \quad (15)$$

$$d^{(j)}=d_{\text{rf}}^{(j)}\left(1+\left\lfloor\frac{B}{1-\delta}\left(1-R_c\right)\right\rfloor\right) \qquad \delta<R<1. \quad (16)$$

Otherwise, if $i<j$ then the SNR exponent is

$$d^{(j)}=d_{\text{rf}}^{(j)}\left(1+\left\lfloor\frac{B}{1-\delta}\left(1-\delta-R_c\right)\right\rfloor\right) \quad 0<R_c\leq 1-\delta. \quad (17)$$

$$d^{(i)}=d_{\text{fso}}^{(i)}\left(1+\left\lfloor\frac{A}{\delta}\left(1-R_c\right)\right\rfloor\right) \qquad 1-\delta<R_c<1 \quad (18)$$

Proof: See Appendix C. ∎

Theorem 4.2 shows how the overall performance of the hybrid channel will be affected when one of the component channels has an asymptotic outage probability that decays with SNR much faster than the other. In particular, we see that the overall SNR exponent will be dominated by the worst of the two component channel SNR exponents unless the binary code rate is below a certain threshold dependent on the ratio of FSO bits to total transmitted bits (δ). Note that these exponents are related to how outage-approaching codes should be designed [34].

To demonstrate the implications of our asymptotic results, we conducted a number of Monte Carlo simulations. This involved computing the mutual information curves $I_{\mathcal{X}_{\text{fso}}}(u)$ and $I_{\mathcal{X}_{\text{rf}}}(u)$ for a given constellation. These curves are then used as look-up-tables to determine the total mutual information (6) for a given set of vector fading realisations $\boldsymbol{h}$ and $\hat{\boldsymbol{h}}$, which are generated randomly according to one of the distributions listed in Table I. The simulation results are shown in Fig. 3. In this example we chose $A=B=1$, $n=4$ (hence $\gamma=4$), 2PPM for the FSO channel and 16QAM for the RF channel. Therefore $m=nq=4$ bits, and a maximum of 8 bits per hybrid channel symbol can be transmitted ($\delta=0.5$). For simplicity we have chosen $\hat{\rho}=1-\rho$. The dot-dashed and dashed curves illustrate the case when only the FSO and RF channels are available, i.e. when $\rho=1$ and $\rho=0$ respectively, and must support $R=3$ bits per symbol. The solid and dot marked curves show the hybrid channel outage performance to support a $R_c=3/8$ and $R_c=6/8$ binary code rate respectively when $\rho=0.5$. In Fig. 3(a), both FSO and RF channels experience exponential scintillation, corresponding to very strong turbulence conditions. In this case, $d_{\text{fso}}^{(1)}=d_{\text{rf}}^{(1)}=1$ and hence Corollary 4.1 applies. As expected the dashed and dot-dashed curves have the same slope since they both have the same SNR exponent. When $R_c=3/8<\delta$, we see the slope of the outage curve becomes steeper when both channels are available (solid curve), in fact the SNR exponent is now $d^{(1)}=2$. However, when $R_c=6/8>\delta$ (dot-marked curve), from (14) the exponent is $d^{(1)}=1$, and hence the curve has the same slope as the FSO and RF only cases previously described. Fig. 3(b) shows the case when the FSO channel now experiences gamma-gamma scintillation with $a=2$ and $b=3$, therefore $d_{\text{fso}}^{(1)}=2$. When $R_c=3/8$ the system benefits from both channels, the overall exponent increases to $d^{(1)}=3$. However, as predicted by our asymptotic results, if $R_c=6/8$ the overall exponent is dominated by the RF component and the exponent is $d^{(1)}=1$. Fig 3(c) shows the case when the FSO and RF channels experience exponential and lognormal scintillation (with $\mu=-\log(2)/2$ and $\sigma^2=\log(2)$) respectively. From Table I, $d_{\text{fso}}^{(1)}=1$ and $d_{\text{rf}}^{(2)}=\frac{1}{4\sigma^2}$. Hence Theorem 4.2 applies in this case. In particular, for the $R_c=3/8$ system, from (17), the hybrid channel exponent is dominated by the RF channel exponent and hence the hybrid outage curve (solid) has the same asymptotic slope as the RF outage curve (dashed). If the required rate is increased to $R_c=6/8$, the exponent is now given by (18), hence the exponent of the FSO channel dominates overall hybrid channel performance. This behaviour can be seen in Fig. 3(c), where the dot marked curve (corresponding to the $R_c=6/8$ hybrid case) has the same slope as the FSO channel (dot-dashed curve). Fig. 3(d) illustrates the case when both channels experience lognormal scintillation corresponding to weak turbulence conditions. In

[5]Note that for the stand-alone FSO system with A blocks, the exponent is given by $d^{(k)}=d_{\text{fso}}^{(k)}(1+\lfloor A(1-R_c/\delta)\rfloor)$ for $0<R_c<\delta$, since we have defined R_c with respect to the hybrid system.

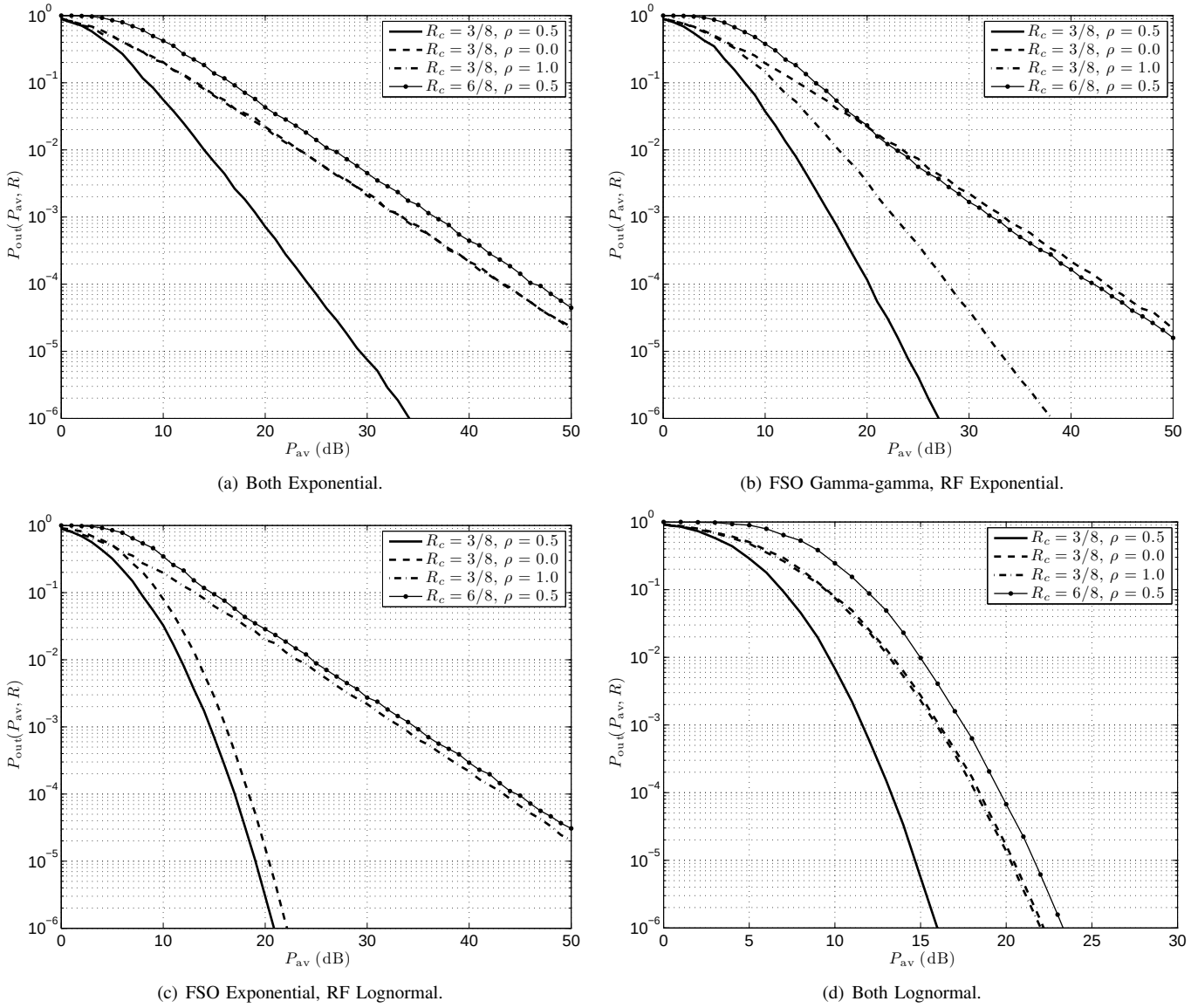

(a) Both Exponential.

(b) FSO Gamma-gamma, RF Exponential.

(c) FSO Exponential, RF Lognormal.

(d) Both Lognormal.

Fig. 3. Outage performance of the hybrid FSO/RF channel with $A = B = 1$, $n = 4$ ($\gamma = 4$), 2PPM FSO and 16QAM RF: solid, dashed and dot-dashed curves correspond to hybrid channel with $R_c = 3/8$ for $\rho = 0.5, 0, 1$ respectively (where $\hat{\rho} = 1 - \rho$). The dot-marked curves show the hybrid outage performance with $R_c = 6/8$ and $\rho = 0.5$.

this case, $d_{\rm fso}^{(2)} = d_{\rm rf}^{(2)} = \frac{1}{4\sigma^2}$, and we see that when $R_c = 3/8$ the hybrid channel benefits from both component channel exponents.

V. Asymptotic Outage Analysis: CSIT Case

In this section we assume both the transmitter and receiver have perfect knowledge of the FSO and RF fading coefficients. Due to the slow nature of the scintillation processes, this is a realistic assumption, which, as we shall see, induces significant power gains. In this case the transmitter adapts the power (subject to power constraints) to compensate for channel fluctuations to significantly reduce the outage probability.

A. Power Allocation Strategies

To find the optimal power allocation strategy, we require the solution to the following minimisation problem.

$$\begin{cases} \text{Minimise:} & \Pr\left\{ I_{\rm tot}(\boldsymbol{p}, \hat{\boldsymbol{p}}, \boldsymbol{h}, \hat{\boldsymbol{h}}) < R \right\} \\ \text{Subject to:} & \mathbb{E}[\langle \boldsymbol{p} \rangle] + \mathbb{E}[\langle \hat{\boldsymbol{p}} \rangle] \leq P_{\rm av}, \\ & \langle \boldsymbol{p} \rangle \leq P_{\rm peak}^{\rm fso},\ \ \langle \hat{\boldsymbol{p}} \rangle \leq P_{\rm peak}^{\rm rf} \end{cases} . \tag{19}$$

Theorem 5.1: The solution to problem (19) is given by

$$(\wp^*, \hat{\wp}^*) = \begin{cases} (\wp, \hat{\wp}) & \langle \wp \rangle + \langle \hat{\wp} \rangle \leq s^* \\ (\mathbf{0}, \mathbf{0}) & \text{otherwise,} \end{cases} \tag{20}$$

where $(\wp, \hat{\wp})$ is the solution to the following minimisation

problem.

$$\begin{cases} \text{minimise} & \langle \boldsymbol{p} \rangle + \langle \hat{\boldsymbol{p}} \rangle \\ \text{subject to} & I_{\text{tot}}(\boldsymbol{p}, \hat{\boldsymbol{p}}, \boldsymbol{h}, \hat{\boldsymbol{h}}) \geq R \\ & \langle \boldsymbol{p} \rangle \leq P_{\text{peak}}^{\text{fso}}, \langle \hat{\boldsymbol{p}} \rangle \leq P_{\text{peak}}^{\text{rf}} \\ & \boldsymbol{p}, \hat{\boldsymbol{p}} \succeq \boldsymbol{0} \end{cases} \tag{21}$$

In (20), s^* is a threshold determined by

$$s^* = \sup \left\{ s : \mathbb{E}_{(\boldsymbol{h}, \hat{\boldsymbol{h}}) \in \mathcal{R}(s)} \left[\langle \wp \rangle + \langle \hat{\wp} \rangle \right] \leq P_{\text{av}} \right\}, \tag{22}$$

where

$$\mathcal{R}(s) \triangleq \left\{ (\boldsymbol{h}, \hat{\boldsymbol{h}}) \in \mathbb{R}^{A+B} : \langle \wp \rangle + \langle \hat{\wp} \rangle \leq s \right\}. \tag{23}$$

Proof: The proof follows similar arguments described in [35, 36]. Essentially, (21) gives the minimum set of power allocations that satisfy the peak power constraints such that total mutual information is greater than the rate requirement. The inclusion of threshold s^* ensures that the long-term power constraint is also satisfied. The larger s^* is, the smaller the outage probability will be. Since the solution $(\wp, \hat{\wp})$ from (21) gives the minimum sum power to satisfy the rate constraint, then this solution also gives the maximum s^*, which in turn minimises the outage probability. ∎

Unfortunately, (21) does not lend itself to a simple solution, since in general $I_{\mathcal{X}}^{\text{awgn}}(p^2)$ is not a concave function in p for all $p > 0$. Thus (21) is a non-convex optimisation problem [37]. Instead of solving (21), we propose a suboptimal algorithm that, as we shall see, exhibits the same asymptotic behaviour as the optimal solution. In this direction, first consider the following lemmas. The proofs follow straightforwardly via the Karush-Kahn-Tucker conditions [37] and using the relationship between mutual information and the minimum mean-square error (MMSE) for Gaussian channels [38], as done in [39].

Lemma 5.1: Define the minimisation problem,

$$\begin{cases} \text{minimise} & \langle \boldsymbol{p}^2 \rangle + \langle \hat{\boldsymbol{p}}^2 \rangle \\ \text{subject to} & I_{\text{tot}}(\boldsymbol{p}, \hat{\boldsymbol{p}}, \boldsymbol{h}, \hat{\boldsymbol{h}}) \geq R \\ & \boldsymbol{p}, \hat{\boldsymbol{p}} \succeq \boldsymbol{0}, \end{cases} \tag{24}$$

where $\langle \boldsymbol{p}^2 \rangle \triangleq \frac{1}{A} \sum_{a=1}^{A} p_a^2$. The solution to (24) is

$$p_a^* = \sqrt{\Upsilon_{\mathcal{X}_{\text{fso}}} \left(h_a^2 \rho^2, \frac{1}{n\lambda} \right)} \quad \text{and} \quad \hat{p}_b^* = \Psi_{\mathcal{X}_{\text{rf}}} \left(\hat{\rho} \hat{h}_b \gamma, \lambda \right), \tag{25}$$

where $\Upsilon_{\mathcal{X}}(u,t) \triangleq \frac{1}{u} \mathsf{mmse}_{\mathcal{X}}^{-1} \left(\min \left\{ \mathsf{mmse}_{\mathcal{X}}(0), \frac{t}{u} \right\} \right)$, $\Psi_{\mathcal{X}}(u,t)$ is the solution x to the equation $\mathsf{mmse}_{\mathcal{X}}(xu) = \frac{2x}{tu}$, $\mathsf{mmse}_{\mathcal{X}}(p)$ denotes the MMSE of a Gaussian channel with discrete input constellation $\mathcal{X}$, $\mathsf{mmse}_{\mathcal{X}}^{-1}(u)$ is the inverse MMSE function, and λ is chosen such that $I_{\text{tot}}(\boldsymbol{p}, \hat{\boldsymbol{p}}, \boldsymbol{h}, \hat{\boldsymbol{h}}) = R$.

Lemma 5.2: Define the minimisation problem

$$\begin{cases} \text{minimise} & \langle \boldsymbol{p}^2 \rangle + \langle \hat{\boldsymbol{p}}^2 \rangle \\ \text{subject to} & I_{\text{tot}}(\boldsymbol{p}, \hat{\boldsymbol{p}}, \boldsymbol{h}, \hat{\boldsymbol{h}}) \geq R \\ & \sqrt{\langle \boldsymbol{p}^2 \rangle} \leq P_{\text{peak}}^{\text{fso}}, \sqrt{\langle \hat{\boldsymbol{p}}^2 \rangle} \leq P_{\text{peak}}^{\text{rf}} \\ & \boldsymbol{p}, \hat{\boldsymbol{p}} \succeq \boldsymbol{0} \end{cases} \tag{26}$$

Let $\boldsymbol{p}^*$ and $\hat{\boldsymbol{p}}^*$ be the solution to (24) in Lemma 5.1, and $\wp$ and $\hat{\wp}$ be the solution to (26). The solution to (26) is separated into four cases depending on $\boldsymbol{p}^*$ and $\hat{\boldsymbol{p}}^*$.

1) If $\boldsymbol{p}^*$ and $\hat{\boldsymbol{p}}^*$ satisfy the constraints in (26). Then $\wp = \boldsymbol{p}^*$ and $\hat{\wp} = \hat{\boldsymbol{p}}^*$.
2) If $\sqrt{\langle (\boldsymbol{p}^*)^2 \rangle} \leq P_{\text{peak}}^{\text{fso}}$ and $\sqrt{\langle (\hat{\boldsymbol{p}}^*)^2 \rangle} > P_{\text{peak}}^{\text{rf}}$. Then

$$\wp_a = \sqrt{\Upsilon_{\mathcal{X}_{\text{fso}}} \left(h_a^2 \rho^2, \frac{1}{n\lambda_1} \right)} \text{ and } \hat{\wp}_b = \Psi_{\mathcal{X}_{\text{rf}}} \left(\hat{h}_b \gamma \hat{\rho}, \lambda_2 \right) \tag{27}$$

where λ_2 is chosen such that $\sqrt{\langle \hat{\wp}^2 \rangle} = P_{\text{peak}}^{\text{rf}}$ and λ_1 is chosen such that

$$\frac{n}{A} \sum_{a=1}^{A} I_{\mathcal{X}_{\text{fso}}}^{\text{awgn}}(\rho^2 h_a^2 \wp_a^2) = R - \frac{1}{B} \sum_{b=1}^{B} I_{\mathcal{X}_{\text{rf}}}^{\text{awgn}}(\hat{\wp}_b \hat{h}_b \hat{\rho} \gamma).$$

If $\sqrt{\langle \wp^2 \rangle} > P_{\text{peak}}^{\text{fso}}$ then the solution to (26) is infeasible.
3) If $\sqrt{\langle (\boldsymbol{p}^*)^2 \rangle} > P_{\text{peak}}^{\text{fso}}$ and $\sqrt{\langle (\hat{\boldsymbol{p}}^*)^2 \rangle} \leq P_{\text{peak}}^{\text{rf}}$. Then the solution to (26) is the same as the previous case, with the roles of rf and fso interchanged.
4) If $\sqrt{\langle (\boldsymbol{p}^*)^2 \rangle} > P_{\text{peak}}^{\text{fso}}$ and $\sqrt{\langle (\hat{\boldsymbol{p}}^*)^2 \rangle} > P_{\text{peak}}^{\text{rf}}$, then the solution to (26) is infeasible.

Comparing (21) with (26), we see that (26) is minimising the sum of the mean-square power of the FSO and RF channels, subject to individual short-term root mean-square (RMS) power constraints. By applying Jensen's inequality [23] to these constraints, we see that a solution to (26) will also satisfy the constraints in (21) and hence can be considered a suboptimal solution to (21). Therefore to find a suboptimal solution to the original minimisation problem (19) we use the solutions in Lemma 5.2 for $(\wp, \hat{\wp})$ instead of solving (21).

B. Asymptotic Analysis

The asymptotic outage performance of optimal power allocation for discrete-input block-fading AWGN channels was analysed by Nguyen *et al.* in [35, 40]. In particular, from [35, Prop. 3], if the peak-to-average power ratios α_{fso} and α_{rf} are finite, then the SNR exponent will be the same as the CSIR case given in Theorems 4.1 and 4.2. When there are no peak-to-average power constraints then the SNR exponent of the optimal power allocation strategy is [40, Th. 2]

$$d_{\text{csit}}^{(1)} = \begin{cases} \infty & d_{\text{csir}}^{(1)} > 1 \\ \frac{d_{\text{csir}}^{(1)}}{1 - d_{\text{csir}}^{(1)}} & d_{\text{csir}}^{(1)} < 1, \end{cases} \tag{28}$$

where $d_{\text{csir}}^{(1)}$ is the SNR exponent for the CSIR case. We now prove that the SNR exponent of our suboptimal power allocation strategy in Section V-A is the same as (28).

Theorem 5.2: Suppose $\alpha_{\text{fso}}, \alpha_{\text{rf}} \to \infty$. Then the SNR exponent of the suboptimal power allocation scheme described by (19) with (26) is given by (28).

Proof: A sketch of proof proceeds as follows. Let $(\boldsymbol{p}^*, \hat{\boldsymbol{p}}^*)$ solve (24). Now consider the following power allocation rule

$$(\wp^\dagger, \hat{\wp}^\dagger) = \begin{cases} (\boldsymbol{p}^*, \hat{\boldsymbol{p}}^*) & \sqrt{\langle (\boldsymbol{p}^*)^2 \rangle + \langle (\hat{\boldsymbol{p}}^*)^2 \rangle} \leq s^\dagger \\ (\boldsymbol{0}, \boldsymbol{0}) & \text{otherwise,} \end{cases} \tag{29}$$

where $s^\dagger$ is a threshold such that $\mathbb{E}_{(\boldsymbol{h},\hat{\boldsymbol{h}})\in\mathcal{R}(s)}\left[\sqrt{\langle \boldsymbol{p}^2\rangle + \langle \hat{\boldsymbol{p}}^2\rangle}\right] = P_{\rm av}$ and

$$\mathcal{R}(s) \triangleq \left\{(\boldsymbol{h},\hat{\boldsymbol{h}}) \in \mathbb{R}^{A+B} : \sqrt{\langle \boldsymbol{p}^2\rangle + \langle \hat{\boldsymbol{p}}^2\rangle} \leq s\right\}. \quad (30)$$

Using similar arguments as [40] it can be proved that the hybrid system with power allocation rule (29) has diversity (28). This diversity lower bounds the diversity achieved by the suboptimal algorithm (19) with (26), since (29) satisfies more stringent power constraints. Hence we conclude the suboptimal power allocation algorithm also has diversity (28). ■

The implications of (28) are described as follows. When $d^{(1)}_{\rm csit} = \infty$, then the outage probability curve will be vertical at a certain threshold of average power, i.e. the hybrid system is able to maintain a constant level of instantaneous input-output mutual information. The threshold at which this occurs is referred to as the *delay-limited capacity* of the system [41]. Note that if $d^{(1)}_{\rm csir} = 1$ in (28) then $d^{(1)}_{\rm csit} = \infty$, however, the outage curve will not go vertical, nor will it converge to a constant slope when plotted on a log-log scale [35]. When the peak-to-average power ratios are finite, the peak power constraints introduce an error floor with a slope equal to the CSIR case. The height of the error floor is dependent on $\alpha_{\rm fso}$ and $\alpha_{\rm rf}$ [35].

To demonstrate the benefits of power allocation and its asymptotic behaviour, we simulated the suboptimal hybrid power allocation strategy for a $A = B = 1$, $n = 4$, 2PPM FSO and 16QAM RF system with $\rho = \hat{\rho} = 0.5$ and peak-to-average power ratios $\alpha_{\rm fso} = \alpha_{\rm rf} = \alpha$. Exponential distributed fading was applied to both channels. Fig. 4(a) shows the hybrid outage performance with our suboptimal power allocation strategy compared to uniform power allocation (cross marked curve) when $R_c = 3/8$. Since, from Corollary 4.1, $d^{(1)}_{\rm csir} = 2$, then from (28), the SNR exponent is $d^{(1)}_{\rm csit} = \infty$, i.e. when there are no peak power constraints, the curve will go vertical at a certain average power threshold. This can be seen in Fig. 4(a) (thick solid curve), for $P_{\rm av} > 8$ dB outages are completely removed. We see that there is a power saving of more than 20 dB compared to uniform power allocation to achieve 10^{-5} outage probability. When peak power constraints are introduced, as expected, we see that an error floor is introduced with the same slope as the CSIR case. The floor shifts down in probability as the peak-to-average power ratio increases. Fig. 4(b) shows the case when $R_c = 6/8$. Since $d^{(1)}_{\rm csir} = 1$, when there are no peak power constraints, the outage curve will no longer go vertical (thick solid curve). As expected we see an error floor is introduced when the peak-to-average power ratio is finite. Nonetheless, we still see significant power savings compared to uniform power allocation.

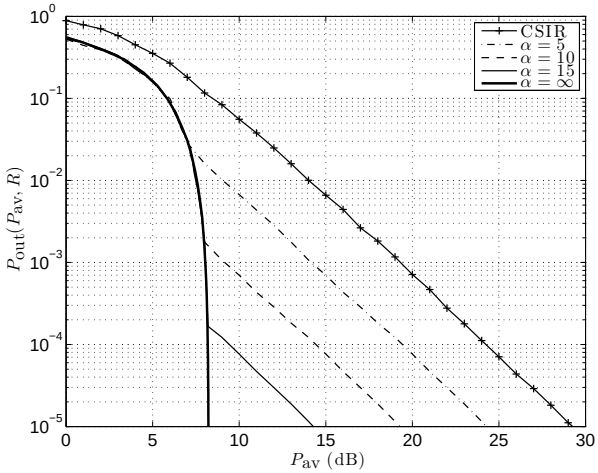

(a) $R_c = 3/8$.

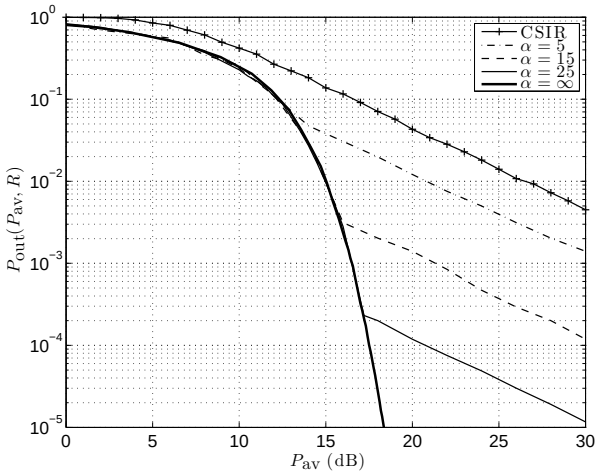

(b) $R_c = 6/8$.

Fig. 4. Outage performance of the hybrid FSO/RF channel with CSIT (solid) and uniform power allocation (dashed). System parameters included: $\rho = \hat{\rho} = 0.5$, $A = B = 1$, $n = 4$, 2PPM FSO and 16QAM RF with peak and average power constraints, and peak-to-average power ratios $\alpha_{\rm fso} = \alpha_{\rm rf} = \alpha$ in decibels. Exponential distributed fading on both channels.

VI. Conclusions

We proposed a simple hybrid FSO/RF channel model based on parallel block fading channels. This hybrid model takes into account differences in signalling rates and fading effects typically experienced by the component channels involved. Under this framework, we examined the information theoretic limits of the hybrid channel. In particular, we studied its asymptotic high SNR outage performance by analysing the outage diversity or SNR exponents. When CSI is only available at the receiver, in the general case, the exponent is not available in closed form. Instead, we derived simple expressions from which it can be computed numerically. For the special case when transmission consists of single FSO and RF blocks, we derived the SNR exponent in closed form in terms of each component channel's SNR exponent, the ratio component channel bits to total bits, and the overall binary code rate of the system. The highest outage diversity is achieved if the hybrid binary code rate is set less than the minimum of the two component channel's maximum binary code rates. At the other extreme, if the hybrid binary code rate is set larger than the maximum of the two component channel's maximum binary code rates, then the SNR exponent is

dominated by the worst of the two component channel's SNR exponents. When CSI is also available at the transmitter, we derived the optimal power allocation scheme that minimises the outage probability subject to peak and average power constraints. Due to the power scaling of the FSO channel, this requires the solution to a non-convex optimisation problem, which is intractable in practical systems. We proposed a suboptimal power allocation strategy, which is much simpler to implement and has the same SNR exponent as the optimal power allocation. Our results indicate that significant power savings (on the order of tens of dBs) are achievable using the suboptimal algorithm compared to uniform power allocation. Future extensions to the work presented in this paper include: asymptotic analysis with a joint distribution on parameters ρ and $\hat{\rho}$; independent non-identically distributed fading; adaptive coding and modulation; practical outage-approaching code design; and lower complexity power adaptation strategies.

ACKNOWLEDGEMENT

We thank Professor Robert Schober and the anonymous reviewers for their helpful comments and suggestions that have significantly improved this work.

APPENDIX A
PROOF OF THEOREM 4.1

Under uniform power allocation, $p_1 = \ldots = p_A = \hat{p}_1 = \ldots = \hat{p}_B = p = P_{\text{av}}$. Define the normalised fading coefficients

$$\zeta_a \triangleq -\frac{\log(h_a^2)}{\log p}, \qquad \xi_b \triangleq -\frac{\log(\hat{h}_b^2)}{\log p}. \tag{31}$$

Assume the FSO and RF component channels have SNR exponents $d_{\text{fso}}^{(k)}$ and $d_{\text{rf}}^{(k)}$ as defined in (9) and (10) respectively. This implies[6]

$$f_\zeta(\zeta) \doteq \exp\left(-d_{\text{fso}}^{(k)}\zeta(\log p)^k\right), \tag{32}$$

$$f_\xi(\xi) \doteq \exp\left(-d_{\text{rf}}^{(k)}\xi(\log p)^k\right), \tag{33}$$

and hence

$$f(\boldsymbol{\zeta},\boldsymbol{\xi}) \doteq \exp\left(-(\log p)^k\left(d_{\text{fso}}^{(k)}\sum_{a=1}^{A}\zeta_a + d_{\text{rf}}^{(k)}\sum_{b=1}^{B}\xi_b\right)\right). \tag{34}$$

In the large SNR limit, the total instantaneous mutual information becomes

$$\lim_{p\to\infty} I_{\text{tot}}(\boldsymbol{p},\hat{\boldsymbol{p}},\boldsymbol{h},\hat{\boldsymbol{h}}) = \frac{nq}{A}\sum_{a=1}^{A}(1-\mathbb{1}\{\zeta_a>1\}) + \frac{m}{B}\sum_{b=1}^{B}(1-\mathbb{1}\{\xi_b>1\}), \tag{35}$$

[6]Note that $g(z) \doteq \exp(-d\log z)$ indicates that $\lim_{z\to\infty} -\frac{\log g(z)}{\log z} = d$.

where $\mathbb{1}\{\cdot\}$ denotes the indicator function. Define the outage set

$$\mathcal{O} \triangleq \left\{\boldsymbol{\zeta},\boldsymbol{\xi} : \frac{nq}{A}\sum_{a=1}^{A}(1-\mathbb{1}\{\zeta_a>1\}) + \frac{m}{B}\sum_{b=1}^{B}(1-\mathbb{1}\{\xi_b>1\}) < R\right\}. \tag{36}$$

Hence we may write the outage probability as

$$P_{\text{out}}(p,R) = \int_{\mathcal{O}} f(\boldsymbol{\zeta},\boldsymbol{\xi})d\boldsymbol{\zeta}d\boldsymbol{\xi}. \tag{37}$$

From the SNR exponent definition (8), using (34) and Varadhan's lemma [42] we have

$$d^{(k)} = \inf_{\mathcal{O}}\left(d_{\text{fso}}^{(k)}\sum_{a=1}^{A}\zeta_a + d_{\text{rf}}^{(k)}\sum_{b=1}^{B}\xi_b\right). \tag{38}$$

Let $0 \le \kappa_1 \le A$ and $0 \le \kappa_2 \le B$ be the number elements of $\boldsymbol{\zeta}$ and $\boldsymbol{\xi}$ set to one respectively. Dividing both sides of the inequality in (36) by $m+nq$ we obtain the set $\mathcal{K}(\delta,R_c)$ as defined in (12), and the infimum (38) is now (11), as given in the theorem.

APPENDIX B
PROOF OF COROLLARY 4.1

Proof: From Theorem 4.1 we must find the infimum (11) over the set

$$\mathcal{K}(\delta,R_c) \triangleq \{\kappa_1,\kappa_2 \in (0,1) : \delta\kappa_1 + (1-\delta)\kappa_2 > 1-R_c\}. \tag{39}$$

Possible solutions to κ_1 and κ_2 include: (a) $\kappa_1=\kappa_2=1$, $d^{(k)} = d_{\text{fso}}^{(k)} + d_{\text{rf}}^{(k)}$, $0 < R_c < 1$; (b) $\kappa_1=1$, $\kappa_2=0$, $d^{(k)} = d_{\text{fso}}^{(k)}$, $1-\delta < R_c < 1$; (c) $\kappa_1=0$, $\kappa_2=1$, $d^{(k)} = d_{\text{rf}}^{(k)}$, $\delta < R_c < 1$. Now suppose $\delta \le \frac{1}{2}$, then $\delta \le 1-\delta$, hence: for $0 < R_c \le \delta$ only solution (a) is possible, therefore $d^{(k)} = d_{\text{fso}}^{(k)} + d_{\text{rf}}^{(k)}$; for $\delta < R_c \le 1-\delta$ solutions (a) and (c) are valid, hence taking the infimum results in $d^{(k)} = d_{\text{rf}}^{(k)}$; for $1-\delta < R_c < 1$, solutions (a), (b) and (c) are valid, and hence the resulting infimum is $d^{(k)} = \min(d_{\text{fso}}^{(k)}, d_{\text{rf}}^{(k)})$. The case when $\delta \ge \frac{1}{2}$ follows similar arguments. ■

APPENDIX C
PROOF OF THEOREM 4.2

The proof follows the same arguments as the proof of Theorem 4.1. First we define the normalised fading coefficients ζ_a and ξ_b as in (31). From (9) and (10) we have

$$f(\boldsymbol{\zeta},\boldsymbol{\xi}) \doteq \exp\left(-(\log p)^i d_{\text{fso}}^{(i)}\sum_{a=1}^{A}\zeta_a - (\log p)^j d_{\text{rf}}^{(j)}\sum_{b=1}^{B}\xi_b\right). \tag{40}$$

From the SNR exponent definition (8), using (34) and Varadhan's lemma [42] we have

$$d^{(i)} = \inf_{\mathcal{K}(\delta,R_c)}\left(d_{\text{fso}}^{(k)}\kappa_1 + (\log p)^{j-i}d_{\text{rf}}^{(j)}\kappa_2\right). \tag{41}$$

$$d^{(j)} = \inf_{\mathcal{K}(\delta,R_c)}\left((\log p)^{i-j}d_{\text{fso}}^{(k)}\kappa_1 + d_{\text{rf}}^{(j)}\kappa_2\right), \tag{42}$$

where the outage set $\mathcal{K}$ is defined as in (12). Now, if $i > j$, then from (42) we need to set κ_1 as small as possible, whilst satisfying (12). If we set $\kappa_1 = 0$ then we require $\kappa_2 = 1 + \lfloor \frac{B}{1-\delta}(1 - R_c) \rfloor$. Since $\kappa_2 \leq B$, then we can only set $\kappa_1 = 0$ if $R_c > \delta$. In this case the exponent is $d^{(j)} = d_{\text{rf}}^{(j)}(1 + \lfloor \frac{B}{1-\delta}(1 - R_c) \rfloor$. If $0 < R_c \leq \delta$ then we must choose $\kappa_1 > 0$. In this case we set $\kappa_2 = B$ and hence to satisfy (12) we require $\kappa_1 = 1 + \lfloor \frac{A}{\delta}(\delta - R_c) \rfloor$. Since $i > j$ the SNR exponent of the FSO channel dominates, and the overall SNR exponent becomes $d^{(i)} = 1 + \lfloor \frac{A}{\delta}(\delta - R_c) \rfloor$ as given in the statement of the theorem. The case when $i < j$ follows the same arguments.

REFERENCES

[1] L. C. Andrews and R. L. Phillips, *Laser Beam Propagation through Random Media*, SPIE Press, USA, 2nd edition, 2005.

[2] N. Letzepis and A. Guillén i Fàbregas, "Outage probability of the Gaussian MIMO free-space optical channel with PPM," *IEEE Trans. Commun. (accepted subject to revisions)*, June 2008, http://arxiv.org/abs/0804.0050.

[3] N. Letzepis and A. Guillén i Fàbregas, "Outage probability of the free-space optical channel with doubly stochastic scintillation," *IEEE Trans. Commun. (accepted subject to revisions)*, June 2008.

[4] N. Letzepis, I. Holland, and W. Cowley, "The Gaussian free space optical MIMO channel with Q-ary pulse position modulation," *IEEE Trans. Wireless Commun.*, vol. 7, no. 5, May 2008.

[5] N. Cvijetic, S. G. Wilson, and M. Brandt-Pearce, "Performance bounds for free-space optical MIMO systems with APD receivers in atmospheric turbulence," *IEEE J. Select. Areas. Commun.*, vol. 26, no. 3, pp. 3–12, April 2008.

[6] S. M. Navidpour, M. Uysal, and M. Kavehrad, "BER performance of free-space optical transmission with spatial diversity," *IEEE Trans. Wireless Commun.*, vol. 6, no. 8, pp. 2813–2819, August 2007.

[7] S. G. Wilson, M. Brandt-Pearce, Q. Cao, and J. H. Leveque, "Free-space optical MIMO transmission with Q-ary PPM," *IEEE Trans. Commun.*, vol. 53, no. 8, pp. 1402–1412, Aug. 2005.

[8] K. Chakraborty, "Capacity of the MIMO optical fading channel," in *Proc. IEEE Int. Symp. Inform. Theory*, Adelaide, Sept. 2005, pp. 530–534.

[9] E. J. Lee and V. W. S. Chan, "Part 1: optical communication over the clear turbulent atmospheric channel using diversity," *J. Select. Areas Commun.*, vol. 22, no. 9, pp. 1896–1906, Nov. 2005.

[10] S. M. Haas and J. H. Shapiro, "Capacity of wireless optical communications," *IEEE J. Select. Areas Commun.*, vol. 21, no. 8, pp. 1346–1356, Oct. 2003.

[11] F. Nadeem, B. Flecker, E. Leitgeb, M. S. Awan, and T. Javornik, "Comparing the fog effects on hybrid network using optical wireless and GHz links," in *Proc. Int. Symp. Commun. Sys., Networks and Digital Signal proc.*, Jun. 2008, pp. 278–282.

[12] H. Wu, B. Hamzeh, and M. Kavehrad, "Achieving carrier class availability of FSO link via complementary RF link," in *Proc. 38th Asilomar Conf. Signals, Systems and Computers*, Oct. 2004.

[13] Z. Jia, F. Ao, and Q. Zhu, "BER performance of the hybrid FSO/RF attenuation system," in *Int. Symp. Anten., Prop. & EM Theory*, Sep. 2006.

[14] T. Kamalakis, I. Neokosmidis, A. Tsipouras, S. Pantazis, and I. Andrikopolous, "Hybrid free space optical / millimeter wave outdoor links for broadband wireless access networks," in *Proc. Int. Symp. Personal, Indoor and Mobile Radio Commun.*, Aug. 2007.

[15] S. Vangala and H. Pishro-Nik, "A highly reliable FSO/RF communication system using efficient codes," in *Proc. IEEE Global Commun. Conf.*, 2007.

[16] H. Wu, B. Hamzeh, and M. Kavehrad, "Availability of airbourne hybrid FSO/RF links," in *Proc. SPIE*, 2005, vol. 5819.

[17] T. Moulsley and E. Vilar, "Experimental and theoretical statistics of microwave amplitude scintillations on satellite down-links," *IEEE Trans. Anten. Propag.*, vol. 30, no. 6, pp. 1099–1106, Jan. 1982.

[18] C. E. Mayer, B. E. Jaeger, R. K. Crane, and X. Wang, "Ka-band scintillations: measurements and model predictions," *Proc. IEEE*, vol. 85, no. 6, pp. 936–945, Jun. 1997.

[19] M. S. Alouini, S. A. Borgsmiller, and P. G. Steffes, "Channel characterization and modeling for Ka-band very small aperture terminals," *Proc. IEEE*, vol. 85, no. 6, pp. 981–997, Jun. 1997.

[20] S. A. Khan, A. N. Tawfik, and C. J. Gibbins, "Short-term amplitude scintillations at 97 GHz on 6.5 km urban link," *Electronic Letters*, vol. 36, no. 19, pp. 1654–1656, Aug. 2000.

[21] S. A. Khan, A. N. Tawfik, B. C. Gremont, and C. J. Gibbins, "Long-term amplitude scintillations at 97 GHz on 6.5 km urban link," *Electronic Letters*, vol. 36, no. 16, pp. 1425–1426, Jul. 2000.

[22] I. B. Djordjevic, B. Vasic, and M. A. Neifeld, "Power efficient LDPC-coded modulation for free-space optical communication over the atmospheric turbulence channel," in *Proc. Conf. Optical Fiber Commun. and Nat. Fiber Optic Engineers Conf.*, Feb. 2007.

[23] T. M. Cover and J. A. Thomas, *Elements of Information Theory*, Wiley Series in Telecommunications, 1991.

[24] L. Zheng and D. Tse, "Diversity and multiplexing: A fundamental tradeoff in multiple antenna channels," *IEEE Trans. Inf. Theory*, vol. 49, no. 5, May 2003.

[25] A. Guillén i Fàbregas and G. Caire, "Coded modulation in the block-fading channel: Coding theorems and code construction," *IEEE Trans. Inf. Theory*, vol. 52, no. 1, pp. 262–271, Jan. 2006.

[26] R. M. Gagliardi and S. Karp, *Optical communications*, John Wiley & Sons, Inc., Canada, 1995.

[27] K. Chakraborty, S. Dey, and M. Franceschetti, "Outage capacity of MIMO Poisson fading channels," *IEEE Trans. Inf. Theory*, vol. 54, no. 11, pp. 4887–4907, Nov. 2008.

[28] S. Dolinar, D. Divsalar, J. Hamkins, and F. Pollara, "Capacity of pulse-position modulation (PPM) on Gaussian and Webb channels," *JPL TMO Progress Report 42-142*, Aug. 2000, URL: lasers.jpl.nasa.gov/PAPERS/OSA/142h.pdf.

[29] A. A. Farid and S. Hranilovic, "Outage capacity optimization for free-space optical links with pointing errors," *IEEE Trans. Light. Tech.*, vol. 25, no. 7, pp. 1702–1710, July 2007.

[30] J. Proakis, *Digital Communications*, McGraw-Hill, 1995.

[31] S. Verdú and T. S. Han, "A general formula for channel capacity," *IEEE Trans. Inf. Theory*, vol. 40, no. 4, pp. 1147–1157, Jul. 1994.

[32] E. Malkamaki and H. Leib, "Evaluating the performance of convolutional codes over block fading channels," *IEEE Trans. Inf. Theory*, vol. 45, no. 5, pp. 1643–1646, Jul. 1999.

[33] L. H. Ozarow, S. Shamai and A. D. Wyner, "Information theoretic considerations for cellular mobile radio," *IEEE Trans. Veh. Technol.*, vol. 43, no. 2, pp. 359–378, May 1994.

[34] R. Knopp and P. Humblet, "On coding for block fading channels," *IEEE Trans. Inf. Theory*, vol. 46, no. 1, pp. 1643–1646, July 1999.

[35] K. D. Nguyen, A. Guillén i Fàbregas, and L. K. Rasmusen, "Power allocation for block-fading channels with arbitrary input constellations," *IEEE Trans. Wireless Commun.*, vol. 8, no. 5, pp. 2514–2523, May 2009.

[36] G. Caire, G. Taricco and E. Biglieri, "Optimum power control over fading channels," *IEEE Trans. Inf. Theory*, vol. 45, no. 5, pp. 1468–1489, July 1999.

[37] S. Boyd and L. Vandenberghe, *Convex Optimization*, Cambridge University Press, 2004.

[38] D. Guo, S. Shamai, and S. Verdú, "Mutual information and minimum mean-square error in Gaussian channels," *IEEE Trans. Inf. Theory*, vol. 51, no. 4, pp. 1261–1282, Apr. 2005.

[39] A. Lozano, A. M. Tulino, and S. Verdú, "Optimum power allocation for parallel Gaussian channels with arbitrary input distributions," *IEEE Trans. Inf. Theory*, vol. 52, no. 7, pp. 3033–3051, July 2006.

[40] K. D. Nguyen, A. Guillén i Fàbregas, and L. K. Rasmussen, "Large-SNR outage analysis of power allocation in block-fading channels," *(submitted to) IEEE Trans. Inf. Theory*, May 2008.

[41] S. V. Hanly and D. N. C. Tse, "Multiaccess fading channels. II. delay-limited capacities," *IEEE Trans. Inf. Theory*, vol. 44, no. 7, pp. 2816–2831, Nov. 1998.

[42] A. Dembo and O. Zeitouni, *Large Deviations Techniques and Applications*, Number 38 in Applications of Mathematics. Springer Verlag, 2nd edition, April 1998.

Nick Letzepis (S '03 – M '06) received the B.E. degree in electrical and electronic engineering from Flinders University, Adelaide, South Australia in 1998, and the Ph.D. degree from the Institute for Telecommunications Research (ITR) at the University of South Australia, Adelaide, in 2006.

He worked with DSpace Pty. Ltd. from 1998 to 2002 as a systems/software engineer, specialising in modem and codec design for satellite communications. He is currently a Research Fellow in the Coding and Information Theory Group at the ITR. His research interests include information theory and coding for multiuser/multiantenna communications, random matrix theory, digital modulation and coding for satellite communications, iterative decoding, and free-space optical communications.

PLACE PHOTO HERE

Khoa D. Nguyen (S '06) received the B.E. in Electrical Engineering at the University of Melbourne, Victoria, Australia in 2005. Since 2006, he has been pursuing the Ph.D. degree in electrical engineering at the Institute for Telecommunications Research, University of South Australia, Australia. He was a summer research scholar at the Australian National University in 2004 and held a visiting appointment at University of Cambridge, United Kingdom in 2007. His research interests are in the areas of information theory and error control codes. He has mainly worked on adaptive techniques and theoretical limits of communications with practical constraints.

Albert Guillén i Fàbregas (S '01 – M '05 – SM'09) was born in Barcelona, Catalunya, Spain, in 1974. He received the Telecommunication Engineering Degree and the Electronics Engineering Degree from Universitat Politècnica de Catalunya, Barcelona, Catalunya, Spain, and the Politecnico di Torino, Torino, Italy, respectively, in 1999, and the Ph.D. in Communication Systems from Ecole Polytechnique Fédérale de Lausanne (EPFL), Lausanne, Switzerland, in 2004.

From August 1998 to March 1999, he conducted his Final Research Project at the New Jersey Institute of Technology, Newark, NJ, USA. He was with Telecom Italia Laboratories, Italy, from November 1999 to June 2000 and with the European Space Agency (ESA), Noordwijk, The Netherlands, from September 2000 to May 2001. During his doctoral studies, from 2001 to 2004, he was a Research and Teaching Assistant at Institut Eurcom, Sophia-Antipolis, France. From June 2003 to July 2004, he was a Visiting Scholar at EPFL. From September 2004 to November 2006, he was a Research Fellow at the Institute for Telecommunications Research, University of South Australia, Mawson Lakes, Australia. Since 2007, he has been a Lecturer in the Department of Engineering, University of Cambridge, Cambridge, U.K., where he is also a Fellow of Trinity Hall. He has held visiting appointments at Ecole Nationale Supérieure des Télécommunications, Paris, France, Universitat Pompeu Fabra, Barcelona, Spain, and the University of South Australia, Australia. His research interests are in communication theory, information theory, coding theory, digital modulation, and signal processing techniques with wireless applications.

Dr. Guillén i Fàbregas is currently an Editor of the IEEE TRANSACTIONS ON WIRELESS COMMUNICATIONS . He received a pre-doctoral Research Fellowship of the Spanish Ministry of Education to join ESA. He received the Young Authors Award of the 2004 European Signal Processing Conference EUSIPCO 2004, Vienna, Austria and the 2004 Nokia Best Doctoral Thesis Award in Mobile Internet and 3rd Generation Mobile Solutions from the Spanish Institution of Telecommunications Engineers. He is also a member of the ARC Communications Research Network (ACoRN) and a Junior Member of the Isaac Newton Institute for Mathematical Sciences.